



Contents lists available at ScienceDirect

# Theoretical and Applied Mechanics Letters

journal homepage: [www.elsevier.com/locate/taml](http://www.elsevier.com/locate/taml)

## Review

## Recent development of transient electronics



Huanyu Cheng<sup>\*</sup>, Vikas Vepachedu

Department of Engineering Science and Mechanics, Materials Research Institute, The Pennsylvania State University, University Park, PA 16802, USA

### HIGHLIGHTS

- A number of inorganic materials and their method of application were studied.
- Models of reactive diffusion were presented to predict the dissolution behavior.
- Various encapsulation approaches were explored as a way to extend the lifetime.
- The transient ECG sensor was configured in a stretchable layout.

### ARTICLE INFO

#### Article history:

Received 10 October 2015

Accepted 26 November 2015

Available online 15 January 2016

#### Keywords:

Transient electronics

Model of reactive diffusion

Encapsulation strategy

Multilayer structures

### ABSTRACT

Transient electronics are an emerging class of electronics with the unique characteristic to completely dissolve within a programmed period of time. Since no harmful byproducts are released, these electronics can be used in the human body as a diagnostic tool, for instance, or they can be used as environmentally friendly alternatives to existing electronics which disintegrate when exposed to water. Thus, the most crucial aspect of transient electronics is their ability to disintegrate in a practical manner and a review of the literature on this topic is essential for understanding the current capabilities of transient electronics and areas of future research. In the past, only partial dissolution of transient electronics was possible, however, total dissolution has been achieved with a recent discovery that silicon nanomembrane undergoes hydrolysis. The use of single- and multi-layered structures has also been explored as a way to extend the lifetime of the electronics. Analytical models have been developed to study the dissolution of various functional materials as well as the devices constructed from this set of functional materials and these models prove to be useful in the design of the transient electronics.

© 2016 The Authors. Published by Elsevier Ltd on behalf of The Chinese Society of Theoretical and Applied Mechanics. This is an open access article under the CC BY license (<http://creativecommons.org/licenses/by/4.0/>).

### Contents

1. Introduction.....	21
2. Hydrolysis of semiconducting materials .....	22
3. Model of reactive diffusion for transient materials .....	23
4. Dissolution of the device with bi-layered structures .....	25
5. Conclusion .....	29
Acknowledgments .....	30
References.....	30

## 1. Introduction

While the development of modern electronics has typically been concerned with durable devices that function stably over time, the advent of transient electronics takes an opposite approach; the destruction of the said devices is designed to provide

unique opportunities. Upon exposure to water, transient electronics disintegrate at a predictable rate while releasing biologically and/or environmentally benign end products [1,2]. This ability opens a wide range of applications from bio-degradable electronics to diagnostic/therapeutic implants [3,4]. One can use an electronic component, for instance, as a temporary implant in a patient and allow it to safely dissolve on its own without the need for a second surgery [1,5]. Ultimately, transient electronics can solve the problem of disposing electronics in a safe and convenient manner [6–8].

The defining quality of transient electronics is their ability to dissolve into non-toxic products upon exposure to water and,

<sup>\*</sup> Corresponding author.

E-mail address: [huanyu.cheng@psu.edu](mailto:huanyu.cheng@psu.edu) (H. Cheng).

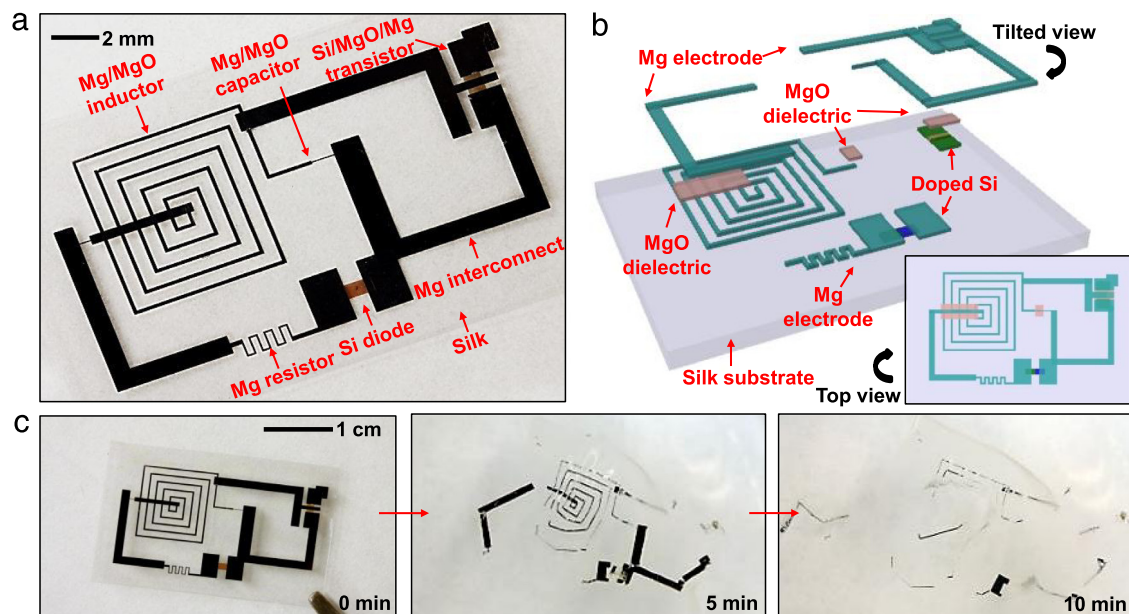


**Fig. 1.** Proof-of-concept demonstration for transient electronics, with key materials and device structure layout. (a) Image of a device with all components deployed on a thin silk substrate. The device components include transistors, diodes, inductors, capacitors, and resistors, with interconnects and interlayer dielectrics. (b) Schematic illustration in an exploded view, with a top view in the lower right inset. (c) Images showing the time sequence at various dissolution stages in deionized (DI) water. Source: Reprinted with permission from Ref. [1].

naturally, dissolution accounts for a significant amount of research in this field [1,2,9–12]. Early research on this topic resulted in achieving the partial dissolution of components through the use of organic materials as substrates [13,14]. For instance, organic thin-film transistors have been developed using cotton-made paper [15] as substrate and silk was also shown to be useful as a soluble substrate for implants in the body [16]. However, this type of research was limited to the substrate and the electronic devices remained insoluble.

More recently however, electronics which are completely soluble have been developed. This relies on a recent, important discovery that semiconductor grade monocrystalline silicon can undergo dissolution in bio-fluids or even water at physiological conditions with a programmed lifetime relevant to applications in biomedicine [1]. As the reaction rate of silicon hydrolysis to form silicic acid ( $\text{Si}(\text{OH})_4$ ) is exceptionally small, silicon devices were fabricated in extremely thin forms. A nanomembrane of silicon with lateral dimensions similar to conventional circuits but with a thickness of 70 nm has been shown to dissolve in  $\sim 10$  days [1]. Via similar chemistry, thin silicon dioxide ( $\text{SiO}_2$ ) was selected as a gate dielectric. Taken together with the other dissolvable, inorganic materials such as magnesium (Mg) and magnesium oxide (MgO) for conductors and the interlayer dielectric, respectively, due to their spontaneous reaction with water to form biologically benign  $\text{Mg}(\text{OH})_2$ , silicon nanomembranes provide a basic means for the construction of a transient, electronic device. As a proof-of-concept, Fig. 1(a) and (b) present a schematic demonstration platform which utilizes silicon nanomembranes (Si NMs) for the semiconductors, magnesium for the conductors, magnesium oxide and silicon dioxide for the dielectrics, and silk for the substrate and packaging materials. The collectively configured devices dissolve and disintegrate when immersed in DI water (Fig. 1(c)).

Surface reactions typically dominate the dissolution behavior for sufficiently large reaction constants. The porosity of the materials (e.g., Mg, MgO and  $\text{SiO}_2$ ) however, was found to be influential as it allows for the diffusion of water through the material, thereby increasing the dissolution rate through an increase in the effective surface area [12]. In studying the dissolution of transient electronics, the factors to consider include

physical and chemical properties of materials, and certain ambient factors of an aqueous environment. Given the research of these factors and others, analytical models have been developed to solidify the understanding of the dissolution behaviors in transient electronics [1,11,12]. Such models can be of great assistance in the design of transient electronics. This review will first provide a comprehensive discussion on the hydrolysis of semiconducting materials with a focus on silicon nanomembranes, followed by the model of reactive diffusion to account for the dissolution behavior of porous materials. When combined with ideas from soft, tissue-like electronic devices, the class of transient electronics provides a viable means to monitor health or deliver care in a minimally obtrusive way.

## 2. Hydrolysis of semiconducting materials

To establish a realistic set of functional materials, knowledge regarding the chemical kinetics of each material is critical, especially that of the hydrolysis of semiconducting materials. At physiological pH levels and temperatures, the dissolution rates of semiconducting materials (e.g., silicon, silicon–germanium, and germanium) are remarkably small [17]. Therefore, in order to minimize the amount of semiconducting materials which must be dissolved, the nanomembrane structure is critical. Dissolution of monocrystalline silicon nanomembranes in phosphate buffered saline (PBS with  $\text{pH} = 7.4$ ) at biologically pertinent temperatures (e.g.,  $37^\circ\text{C}$ ) forms either an intermediate oxidation product  $\text{SiO}_2$  or  $\text{Si}(\text{OH})_4$  through the equilibrium:  $\text{Si} + 4\text{H}_2\text{O} \leftrightarrow \text{Si}(\text{OH})_4 + 2\text{H}_2$  [18,19]. The rate depends on the crystal structure, morphology, and doping concentration of silicon [20,21], as well as the temperature and composition of solutions [2,19].

Systematic characterization of the dissolution kinetics for silicon used various bio-fluids at multiple pH levels and temperatures. Patterned Si NMs ( $3\ \mu\text{m} \times 3\ \mu\text{m} \times 70\ \text{nm}$ ) were first created on a layer of thermal oxide on a silicon wafer, followed by immersion in aqueous buffer solutions (50 mL, in a petri dish with diameter of 7 cm). The dissolution rate of thermal oxide is negligible in comparison to that of silicon. Thicknesses of Si NMs were measured at a specific time (e.g., every other day) after which the sample was

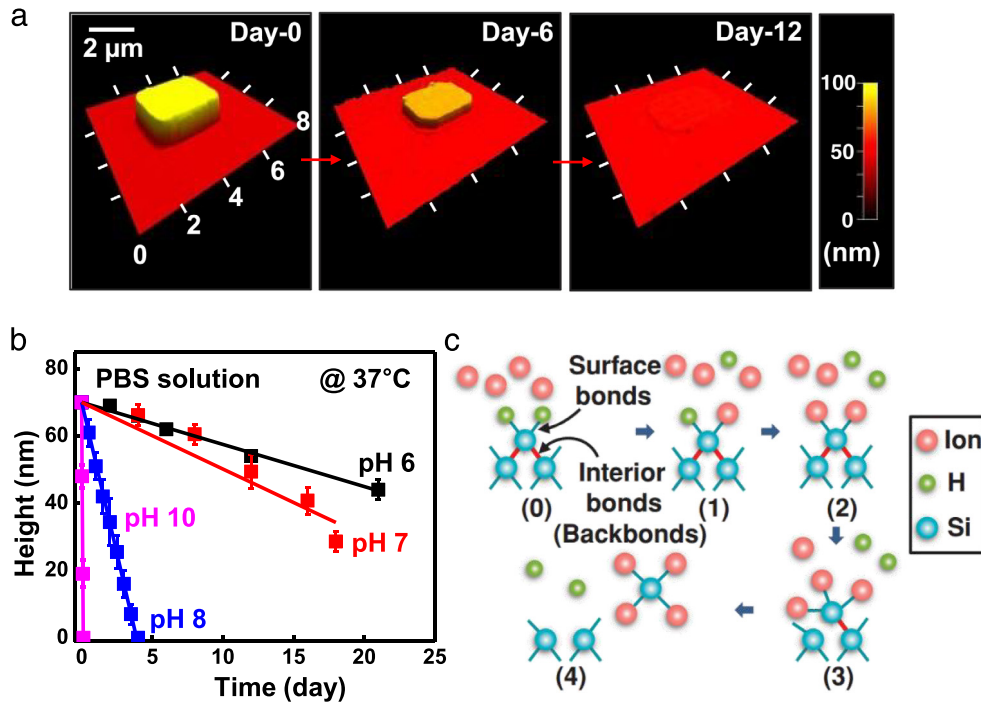


**Fig. 2.** Experiments of silicon dissolution with corresponding theoretical and numerical analyses. (a) Atomic force microscope topographical images of a Si NM with initial dimension of  $3\ \mu\text{m} \times 3\ \mu\text{m} \times 70\ \text{nm}$  at various stages of hydrolysis in PBS at  $37^\circ\text{C}$ . (b) Theoretical (lines) and experimental (symbols) dissolution of Si NMs from (a) in buffer solutions at different pH levels (pH 6, black; pH 7, red; pH 8, blue; pH 10, purple), at physiological temperature ( $37^\circ\text{C}$ ). (c) Atomic configurations for each ion adsorption event in density functional theory (DFT) simulation of the silicon dissolution process. (For interpretation of the references to color in this figure legend, the reader is referred to the web version of this article.)

Source: Figure (a) reprinted with permission from Ref. [1], (b) reprinted with permission from Ref. [2] and (c) reprinted with permission from Ref. [22].

placed into a fresh buffer solution. There was no significant change in the dissolution rate for a variety of time intervals (e.g., for every 1, 2, 4, 7 days), indicating accurate measurement in the dissolution rate. Studies of SiGe and Ge were given in a similar setup [17]. Figure 2(a) presents atomic force microscope topographical images of a Si NM with an initial thickness of 70 nm collected at various stages of hydrolysis, demonstrating its transient behavior in bio-fluids (PBS with pH of 7.4;  $37^\circ\text{C}$ ).

Given the dense arrangement of the silicon atoms in crystal structures, the hydrolysis of monocrystalline silicon nanomembranes is limited to the surface and the kinetics can be described by a surface reaction with a constant dissolution rate [1,2]. With the assumption that no solution molecules diffuse into the silicon, this model yields a linear relationship between the measured thickness and the time, where the slopes represent the dissolution rates. A previously established empirical formula [19] suggests that an increase in the hydroxide ion concentration  $[\text{OH}^-]$  results in an accelerated dissolution rate in high pH solutions of KOH. As shown in Fig. 2(b), this formula can reproduce the experimental trends for solutions at the physiological pH levels if a different power law exponent is used for  $[\text{OH}^-]$  [2].

In conjunction with the pH levels, the type and concentration of ions also have appreciable effects on the dissolution process. Experimental data show the dissolution rate of silicon in bovine serum ( $\approx$ protein  $40\ \text{g} \cdot \text{L}^{-1}$ ,  $\approx 0.12\ \text{M}$  sodium chlorides, pH 7.4 at  $37^\circ\text{C}$ ) is 20 times higher than that in the phosphate buffered saline solution at comparable pH ( $\approx 0.14\ \text{M}$  chlorides and  $0.01\ \text{M}$  phosphates, pH 7.4 at  $37^\circ\text{C}$ ). In an effort to examine the underlying aspects of concentration of anions found in the biological systems such as chlorides ( $\text{Cl}^-$ ) and phosphates ( $\text{HPO}_4^{2-}$ ), studies on dissolution of Si NMs as a function of ion concentration (chlorides and phosphates,  $0.05\ \text{M}$ – $1\ \text{M}$ ) were performed at a pH level fixed at 7.5 [22]. Experimental measurements indicate a power law dependence of dissolution rates on  $[\text{Cl}^-]$  and  $[\text{HPO}_4^{2-}]$ , as for

$[\text{OH}^-]$  in high pH solutions of KOH. A layer by layer dissolution of Si NMs at the surface is an effect of nucleophilic attack by  $\text{OH}^-$  of silicon surface bonds, which weakens the interior bonds of surface silicon. The other anions can also promote the dissolution of Si NMs as they act as nucleophiles. Atomic level simulations show elongated interior bonds of surface silicon after adsorption of  $\text{OH}^-$ ,  $\text{Cl}^-$ , and  $\text{HPO}_4^{2-}$ , suggesting a decrease in their strength. A schematic representation of the ion adsorption process on the silicon surface is shown in Fig. 2(c). With the capability to interact with silicon surface in a manner similar to  $\text{OH}^-$ , nucleophilic anions such as  $\text{Cl}^-$  and  $\text{HPO}_4^{2-}$  assist the dissolution of Si NMs [22].

In order to construct functional devices, the dissolution of doped silicon with different types and concentrations is of importance as well. Consistent with the prior study of silicon dissolution at comparatively high pH levels and temperatures [21], the measurement of Si NMs doped with phosphorus (P) or boron (B) at different concentrations indicates a significant reduction in dissolution rates when dopant concentrations surpass a certain level (e.g.,  $10^{20}\ \text{cm}^{-3}$ ). As described by an empirical expression  $R_{\text{dissolution}} = R_i / [1 + (C/C_0)^4]$ , the dissolution rate remains constant ( $R_i$ ) until a critical dopant concentration ( $C_0$ ) is reached and then the rate decreases sharply. In the empirical expression,  $R_i$  and  $C_0$  depend on temperature following an Arrhenius law with different activation energies. This empirical expression also captures the dissolution behavior of doped silicon in physiologically relevant conditions [20].

### 3. Model of reactive diffusion for transient materials

In addition to surface reactions, the diffusion in the porous materials cannot be ignored and the reaction between the diffused molecules and surrounding porous materials also needs to be considered. A model of reactive diffusion was proposed to analytically study the dissolution process of porous materials [23].

The model considers the diffusion of water and hydroxide ions into porous materials, which effectively increases the reactive surface. Here the key parameters are the diffusivity  $D$  of water in the porous material and the reaction constant  $k$  between water and the material. Because the initial thickness  $h_0$  is much smaller than both the width and length of the sample in the experiment, the one-dimensional (1D) model can adequately capture the dissolution behaviors. With  $y = 0$  at the bottom of the material layer (Fig. 4(a)), the water concentration  $w(y, t)$  at location  $y$  and time  $t$  satisfies the reactive diffusion equation [23]

$$D \frac{\partial^2 w}{\partial y^2} - kw = \frac{\partial w}{\partial t}, \quad 0 \leq y \leq h_0. \quad (1)$$

This equation reduces to the standard diffusion equation if the reaction constant  $k$  is negligible. The boundary conditions of Eq. (1) include a constant water concentration at the water/porous material interface  $w|_{y=h_0} = w_0$  and a zero water flux at the porous material/substrate interface  $\partial w / \partial y|_{y=0} = 0$ . The initial condition is zero water concentration  $w|_{t=0} = 0$  ( $0 \leq y < h_0$ ). In order to transform the inhomogeneous boundary condition  $w|_{y=h_0} = w_0$  to a homogeneous one, a new variable  $\theta = w - w_0$  is introduced [12], which results in an updated equation

$$D \frac{\partial^2 \theta}{\partial y^2} - k\theta - \frac{\partial \theta}{\partial t} = kw_0, \quad 0 \leq y \leq h_0. \quad (2)$$

The boundary conditions and the initial condition become  $\theta|_{y=h_0} = 0$ ,  $\partial \theta / \partial y|_{y=0} = 0$ , and  $\theta|_{t=0} = -w_0$  ( $0 \leq y < h_0$ ), respectively. Eq. (2) is inhomogeneous, but the general solution can be represented by a sum of a homogeneous solution  $\theta_h$  and a particular solution  $\theta_p$ . The homogeneous solution  $\theta_h$  satisfies the homogeneous equation  $D \partial^2 \theta_h / \partial y^2 - k\theta_h - \partial \theta_h / \partial t = 0$  with homogeneous boundary conditions  $\theta_h|_{y=h_0} = 0$  and  $\partial \theta_h / \partial y|_{y=0} = 0$ . Expressed in the form of  $\theta_h = Y(y)T(t)$ ,  $\theta_h$  can be solved by the method of separation of variables. The homogeneous equation leads to  $DY''/Y - k = T'/T = -\lambda$ , where  $\lambda$  is the eigenvalue to be determined from the boundary condition. The functions  $T(t)$  and  $Y(y)$  are then expressed as  $T = e^{-\lambda t}$  and  $Y = A \sin[\sqrt{(\lambda - k)/D}y] + B \cos[\sqrt{(\lambda - k)/D}y]$ , where  $A$  and  $B$  are constants to be determined from initial and boundary conditions. With  $Y|_{y=h_0} = 0$  and  $Y'|_{y=0} = 0$  obtained from the homogeneous boundary conditions,  $A$  is solved to be  $A = 0$  and the trigonometric equation  $\cos[\sqrt{(\lambda - k)/D}h_0] = 0$  leads to the solution for eigenvalues  $\lambda_n = [(2n - 1)\pi / (2h_0)]^2 D + k$  ( $n = 1, 2, 3, \dots$ ), which in turn gives the homogeneous solution

$$\theta_h = \sum_{n=1}^{\infty} \left\{ B_n e^{-\left[\left(\frac{2n-1}{2h_0}\pi\right)^2 D + k\right]t} \cos\left(\frac{2n-1}{2h_0}\pi y\right) \right\}, \quad (3)$$

with constants  $B_n$  to be determined from the initial condition. The particular solution  $\theta_p$  needs to satisfy the inhomogeneous equation and homogeneous boundary conditions. A suitable choice is  $\theta_p = w_0 [\cosh(\sqrt{k/D}y) / \cosh(\sqrt{k/D}h_0) - 1]$ . The substitution of the general solution  $\theta = \theta_h + \theta_p$  in the initial condition leads to  $B_n = 4(-1)^n (2n - 1) \pi D w_0 / [4kh_0^2 + (2n - 1)^2 \pi^2 D]$ , from which the solution of Eq. (1) is obtained as

$$w(y, t) = w_0 \left\{ \frac{\cosh\left(\sqrt{\frac{kh_0^2}{D}} \frac{y}{h_0}\right)}{\cosh\sqrt{\frac{kh_0^2}{D}}} + 2 \sum_{n=1}^{\infty} \frac{(-1)^n (n - \frac{1}{2}) \pi}{\frac{kh_0^2}{D} + (n - \frac{1}{2})^2 \pi^2} e^{-\left[\frac{kh_0^2}{D} + (n - \frac{1}{2})^2 \pi^2\right] \frac{Dt}{h_0^2}} \right\}. \quad (4)$$

The solution given above indicates a clear scaling law  $w/w_0 = \bar{w}(y/h_0, Dt/h_0^2, kh_0^2/D)$  in which the normalized water concentration  $w/w_0$  depends on normalized position  $y/h_0$ , normalized time  $Dt/h_0^2$ , and a single non-dimensional parameter  $kh_0^2/D$  that scales with the ratio of reaction constant  $k$  to diffusivity  $D$ . Experimental measurement of Mg with an initial thickness of 300 nm shows  $D = 6.0 \times 10^{-12} \text{ cm}^2/\text{s}$  and  $k = 1.2 \times 10^{-3} \text{ s}^{-1}$  which is within the range of reaction constants reported by Taub et al. [24]. Figure 3(a) presents the distribution of water concentration for the normalized time  $Dt/h_0^2 = 0.1, 0.2, 0.4, 0.8, 2$  and  $\infty$ , where  $Dt/h_0^2 = \infty$  corresponds to the steady-state limit of the water concentration in the Mg layer  $w(y, t \rightarrow \infty) = w_0 \cosh(\sqrt{kh_0^2/D}y/h_0) / \cosh\sqrt{kh_0^2/D}$ .

Realizing the definition of the reaction constant, the mass of water reacted at a given location (per unit volume) is  $kw$ . When  $q$  water molecules react with one atom of the porous material, the mass of the dissolved porous material (per unit volume) at this location is  $kwM / (qM_{\text{H}_2\text{O}})$ , where  $M$  and  $M_{\text{H}_2\text{O}} = 18 \text{ g} \cdot \text{mol}^{-1}$  are the molar masses of porous material and water, respectively. Integration of  $kwM / (qM_{\text{H}_2\text{O}})$  over both the thickness  $y$  and time  $t$  yields the total dissolved mass of porous material, which in turn gives a scaling law of the remaining thickness  $h$  normalized by its initial thickness  $h_0$ , before complete physical disappearance, as

$$\frac{h}{h_0} = 1 - \frac{w_0 M}{q \rho M_{\text{H}_2\text{O}}} \frac{kh_0^2}{D} \times \left\{ \frac{Dt}{h_0^2} \cdot \frac{\tanh\sqrt{\frac{kh_0^2}{D}}}{\sqrt{\frac{kh_0^2}{D}}} - 2 \sum_{n=1}^{\infty} \frac{1 - e^{-\left[\frac{kh_0^2}{D} + (n - \frac{1}{2})^2 \pi^2\right] \frac{Dt}{h_0^2}}}{\left[\frac{kh_0^2}{D} + (n - \frac{1}{2})^2 \pi^2\right]^2} \right\}, \quad (5)$$

where  $\rho$  is the mass density of the porous material. For parameters  $k$  and  $D$  relevant to applications of transient electronics in biomedicine, the summation on the right hand side of Eq. (5) is negligible in linear expression for the thickness as  $h/h_0 \approx 1 -$

$t/t_c$ , where  $t_c = (h_0/\sqrt{kD}) [q\rho M_{\text{H}_2\text{O}} / (w_0 M)] (\tanh\sqrt{kh_0^2/D})^{-1}$  is the critical time of complete physical disappearance for the transient material. The rate of dissolution  $v_{\text{dissolution}}$ , also known as the electrical dissolution rate used for conductors [25], can be determined from the linear approximation of the thickness as  $v_{\text{dissolution}} = -dh/dt \approx h_0/t_c = \sqrt{kD}w_0M / (q\rho M_{\text{H}_2\text{O}}) \tanh\sqrt{kh_0^2/D}$ . The rate of dissolution is 0.044 nm/s, 0.13 nm/s, and 0.20 nm/s for 100 nm-, 300 nm- and 500 nm-thick Mg layers, respectively. These quantities have the same order of magnitude as rates of dissolution reported in the prior experiments [26,27].

The chemical reaction of Mg in phosphate buffered saline follows  $\text{Mg} + 2\text{H}_2\text{O} \rightarrow \text{Mg}(\text{OH})_2 + \text{H}_2$ . Thus, two water molecules react with one Mg atom (i.e.,  $q = 2$ ). Because water molecules are the dominant molecule in phosphate buffered saline or the other bio-fluids, the water concentration is approximately  $w_0 = 1 \text{ g} \cdot \text{cm}^{-3}$ . The critical time  $t_c$  to dissolve Mg (molar mass  $M = 24 \text{ g} \cdot \text{mol}^{-1}$ , mass density  $\rho = 1.738 \text{ g} \cdot \text{cm}^{-3}$ , and initial thickness  $h_0 = 300 \text{ nm}$ ) is calculated as 38 min, which agrees reasonably well with the measurement of 40 min in the experiment. Via a similar chemistry, one silicon oxide atom reacts with two water molecules by  $\text{SiO}_2 + 2\text{H}_2\text{O} \rightarrow \text{Si}(\text{OH})_4$ . Because the reaction



between SiO<sub>2</sub> and water is much slower than between Mg and water (minutes to dissolve Mg versus days to dissolve SiO<sub>2</sub>), the reaction constant between water and SiO<sub>2</sub> ( $\sim 10^{-6} \text{ s}^{-1}$ ) is much smaller than that between water and Mg ( $\sim 10^{-3} \text{ s}^{-1}$ ). The rates of dissolution range from 0.11 to 0.47 nm/h for SiO<sub>2</sub> with an initial thickness between 35 and 100 nm at a temperature between room and physiological temperatures. These rates of dissolution for PECVD SiO<sub>2</sub> in water are consistent with the rates reported in prior experiments [28], which are higher than those for quartz [29].

In comparison to the intermittent thickness measurement, electrical properties can potentially provide continuous measurements. Electrical measurements also allow for evaluation of the dissolution behavior of a conductive material below a nonconductive layer, as discussed in the next section. The relative changes in both the width and length directions are much smaller than in the thickness direction. Therefore, the electric resistance is inversely proportional to the remaining thickness as  $R = R_0 h_0 / h \approx R_0 / (1 - t/t_c)$ , where  $R_0$  is the initial resistance. Changes of resistance approximately account for both changes in thickness and influences associated with porosity, pitting and other non-uniformities induced by non-uniform dissolution [25]. The normalized electric resistance  $R/R_0$  of Mg is shown in Fig. 4(c) as a function of the normalized time  $t/t_c$ . In this figure, the same reaction constant  $k = 1.2 \times 10^{-3} \text{ s}^{-1}$  and diffusivity  $D = 6.0 \times 10^{-12} \text{ cm}^2/\text{s}$  are chosen for Mg with an initial thickness of 300 nm and initial resistance (per unit length)  $R_0$  of 1.06  $\Omega/\text{mm}$ . It is important to note that an initial layer of thin MgO may exist on top of the Mg layer. In the presence of water, this thin MgO layer quickly reacts to form a more stable, crystalline hydroxide [30], which is not as protective as non-crystalline films [31]. Thus, the single-layer dissolution model can properly account for the hydrolysis of Mg.

The potential of thin films made from other transient metals for use in transient electronics has also been explored and was found to be worth considering with the development of MOSFETs as an example [25]. Analytical models discussed above are found to be applicable to other dissolvable metals, including Mg alloy, zinc (Zn), tungsten (W), and molybdenum (Mo). The prediction from the model can reproduce the observed dissolution behaviors in DI water and simulated body fluids (e.g., Hanks' solution with pH from 5 to 8) [25]. Particularly, the electrical dissolution rates in thin films can be much different from traditionally reported corrosion rates in corresponding bulk materials. The model cannot, however, capture the dissolution behavior of iron (Fe), because Fe degrades in a spatially non-uniform manner, with certain reaction products (Fe<sub>2</sub>O<sub>3</sub> and Fe<sub>3</sub>O<sub>4</sub>) that have very low solubility [25].

Silicon oxides and silicon nitrides are key materials for dielectrics and encapsulation layers in the class of silicon-based high performance electronics. The dissolution rates of these materials are affected by the physical and chemical properties of the films, which in turn depend on the deposition/growth methods and conditions. A key parameter that can approximately characterize these differences is density. The effects of density variation are two-fold. Reduced density increases the porosity in the porous materials, which results in an increased reactive surface to accelerate the dissolution. Secondly, it also reduces the amount of materials that need to be dissolved. The effective density  $\rho_{\text{eff}}$  of porous material is related to the density  $\rho_s$  of the fully dense materials as  $\rho_{\text{eff}} = \rho_s V_s / (V_s + V_{\text{air}})$ , where  $V_s$  and  $V_{\text{air}}$  are the volumes of the porous material and air cavity, respectively. A modified version of the reactive diffusion model provides a simple means to account for the density variation [11]. In Eq. (1), the diffusivity  $D$  is replaced with an effective diffusivity  $D_e$ . The effective diffusivity of water in a porous medium is linearly proportional to the pore fraction in the porous medium:  $D_e \propto V_{\text{air}} / (V_{\text{air}} + V_s) = (\rho_s - \rho_{\text{eff}}) / \rho_s$ . As densities of porous materials from various deposition methods/conditions are measured directly

from the experiment, the effective diffusivity of water in each porous material can be determined. At time  $t = 0$ , the air pores are filled with water, i.e.,  $w|_{t=0} = w_0 (\rho_s - \rho_{\text{eff}}) / \rho_s$  ( $0 \leq y < h_0$ ). The boundary conditions remain the same as those for Eq. (1). Following the same approach discussed above, the normalized thickness is solved as [11]

$$\frac{h}{h_0} = 1 - \frac{w_0 M}{q \rho_{\text{eff}} M_{\text{H}_2\text{O}}} \frac{k h_0^2}{D_e} \left\{ \frac{D_e t \tanh \sqrt{\frac{k h_0^2}{D_e}}}{h_0^2 \sqrt{\frac{k h_0^2}{D_e}}} - 2 \sum_{n=1}^{\infty} C_n \frac{1 - e^{-\left[ \frac{k h_0^2}{D_e} + \left(n - \frac{1}{2}\right)^2 \pi^2 \right] \frac{D_e t}{h_0^2}}}{\left[ \frac{k h_0^2}{D_e} + \left(n - \frac{1}{2}\right)^2 \pi^2 \right]} \right\}, \quad (6)$$

where  $C_n$  is  $C_n = \left[ \frac{k h_0^2}{D_e} + \left(n - \frac{1}{2}\right)^2 \pi^2 \right]^{-1} + (\rho_{\text{eff}} / \rho_s - 1) / \left(n - \frac{1}{2}\right)^2 \pi^2$ . The dissolution rate is then estimated as  $-dh/dt = k h_0 w_0 M / (q \rho_{\text{eff}} M_{\text{H}_2\text{O}}) \tanh \sqrt{k h_0^2 / D_e} / \sqrt{k h_0^2 / D_e}$ . With measured densities and calculated effective diffusivities, the reaction constants are found to be different for silicon oxides (or nitrides) deposited from different conditions as well. The results suggest that the density has affected the dissolution rate through changes in diffusion, as well as through differences in reactivity. Besides the dissolution at a molecular level, the removal of nanoscale pieces of material from the film may also be possible as narrow regions of the porous matrix disappear by hydrolysis. This discovery promises the future development of tunable dissolution through geometrical variations. When combined with patterned structures in the transient materials or the encapsulation layer (to be discussed in the next section), the dissolution behavior of transient electronics may be tuned actively through changes of diffusivity and reactivity from deformation upon stimuli, including swelling, thermal and mechanical loadings.

#### 4. Dissolution of the device with bi-layered structures

Applications in biomedicine require the transient electronics to function stably in a certain timeframe, followed by a complete physical disappearance. All of the transient materials however, start to dissolve immediately in the bio-fluids. The lifetime of the resulting devices is typically determined by Mg interconnects due to their fast reaction with water. Although the system may function before it completely breaks down, its performance is significantly compromised. Therefore, it is important to explore a mechanism that allows devices to function in a programmed lifetime.

Adding encapsulation layers or packaging materials on top of the device can extend its lifetime in a controlled manner. For instance, MgO can serve as an encapsulation layer for Mg. In this bi-layered system (Fig. 4(b)), zero initial condition at  $t = 0$  applies to both Mg and MgO layers. The reactive diffusion Eq. (1) together with zero water flux boundary condition at the bottom surface  $y = 0$  still holds for the Mg layer. As for the MgO encapsulation with an initial thickness of  $h_{\text{encapsulation}}$ , the reactive diffusion equation becomes [12]  $D_{\text{encapsulation}} \frac{\partial^2 w}{\partial y^2} - k_{\text{encapsulation}} w = \frac{\partial w}{\partial t}$  ( $h_0 \leq y \leq h_0 + h_{\text{encapsulation}}$ ), where  $D_{\text{encapsulation}}$  and  $k_{\text{encapsulation}}$  are the diffusivity of water in MgO and reaction constant between MgO and water, respectively. The constant water concentration boundary condition at the MgO/water interface is  $w|_{y=h_0+h_{\text{encapsulation}}} = w_0$ . In addition, the continuity conditions of water concentration and flux across the MgO/Mg interface are  $w|_{y=h_0-0} = w|_{y=h_0+0}$  and  $D \partial w / \partial y|_{y=h_0-0} = D_{\text{encapsulation}} \partial w / \partial y|_{y=h_0+0}$ . Similar to the single-layer system, the

inhomogeneous boundary condition leads to a representation of the water concentration as a sum of a homogeneous solution  $w_h$  and a particular solution  $w_p$ , i.e.,  $w = w_h + w_p$ . The homogeneous solution  $w_h$  satisfies the homogeneous equation  $D' \partial^2 w_h / \partial y^2 - k' w_h = \partial w_h / \partial t$ , where  $D' = D$  and  $k' = k$  for  $0 \leq y \leq h_0$  in the Mg layer, and  $D' = D_{\text{encapsulation}}$  and  $k' = k_{\text{encapsulation}}$  for  $h_0 \leq y \leq h_0 + h_{\text{encapsulation}}$  in the MgO encapsulation. The boundary conditions become homogeneous as well, i.e.,  $w_h|_{y=h_0+h_{\text{encapsulation}}} = 0$ ,  $\partial w_h / \partial y|_{y=0} = 0$ .

By the method of separation of variables, the homogeneous solution is solved as  $w_h = w_0 \sum_{n=1}^{\infty} C_n e^{-\lambda_n t} f_n(y)$ , where the coefficients  $C_n$  are to be determined from the initial condition,  $\lambda_n$  ( $n = 1, 2, 3, \dots$ ) can be solved from the following eigen equation

$$\tan \sqrt{\frac{\lambda - k}{D}} h_0 \tan \sqrt{\frac{\lambda - k_{\text{encapsulation}}}{D_{\text{encapsulation}}}} h_{\text{encapsulation}} = \sqrt{\frac{(\lambda - k_{\text{encapsulation}}) D_{\text{encapsulation}}}{(\lambda - k) D}}, \quad (7)$$

and  $f_n(y)$  is written as

$$f_n(y) \equiv \begin{cases} \sin \left( \sqrt{\frac{\lambda_n - k_{\text{encapsulation}}}{D_{\text{encapsulation}}}} h_{\text{encapsulation}} \right) \\ \times \cos \left( \sqrt{\frac{\lambda_n - k}{D}} y \right), & 0 \leq y \leq h_0, \\ \cos \left( \sqrt{\frac{\lambda_n - k}{D}} h_0 \right) \\ \times \sin \left[ \sqrt{\frac{\lambda_n - k_{\text{encapsulation}}}{D_{\text{encapsulation}}}} (h_0 + h_{\text{encapsulation}} - y) \right], & h_0 \leq y \leq h_0 + h_{\text{encapsulation}}. \end{cases} \quad (8)$$

Satisfying the reactive diffusion equation, together with inhomogeneous boundary condition, zero water flux at the bottom of Mg layer, and continuity conditions, the particular solution  $w_p$  is solved as  $w_p = w_0 g(y)$ , where

$$g(y) \equiv \begin{cases} G \cosh \left( \sqrt{\frac{k}{D}} y \right), & 0 \leq y \leq h_0, \\ \cosh \left( \xi \frac{h_0 + h_{\text{encapsulation}} - y}{h_{\text{encapsulation}}} \right) \\ - H \sinh \left( \xi \frac{h_0 + h_{\text{encapsulation}} - y}{h_{\text{encapsulation}}} \right), & h_0 \leq y \leq h_0 + h_{\text{encapsulation}}, \end{cases} \quad (9a,b)$$

$$G = \frac{1}{\sqrt{\frac{Dk}{D_{\text{encapsulation}} k_{\text{encapsulation}}}} \sinh \sqrt{\frac{kh_0^2}{D}} \sinh \xi + \cosh \sqrt{\frac{kh_0^2}{D}} \cosh \xi}, \quad (10a,b)$$

$$H = \frac{\sqrt{\frac{Dk}{D_{\text{encapsulation}} k_{\text{encapsulation}}}} \tanh \sqrt{\frac{kh_0^2}{D}} + \tanh \xi}{\sqrt{\frac{Dk}{D_{\text{encapsulation}} k_{\text{encapsulation}}}} \tanh \sqrt{\frac{kh_0^2}{D}} \tanh \xi + 1},$$

and  $\xi = \sqrt{k_{\text{encapsulation}} h_{\text{encapsulation}}^2 / D_{\text{encapsulation}}}$ . With the expression of the water concentration  $w = w_0 [\sum_{n=1}^{\infty} C_n e^{-\lambda_n t} f_n(y) + g(y)]$ , the zero initial condition leads to  $\sum_{n=1}^{\infty} C_n f_n(y) + g(y) = 0$ . Orthogonality of eigenfunctions requires  $\int_0^{h_0+h_{\text{encapsulation}}} f_m(y) f_n(y) dy = 0$  (if  $m \neq n$ ), which yields the coefficient  $C_n$  analytically as Eq. (11) given in Box I. The expression given in Eq. (11)

completes the solution of the reactive diffusion equation for bi-layered structures. In addition to the dependence on  $y/h_0$ ,  $Dt/h_0^2$ , and  $kh_0^2/D$  as in the single-layer solution, the normalized water concentration  $w/w_0$  also depends on the normalized reaction constant  $k_{\text{encapsulation}} h_{\text{encapsulation}}^2 / D_{\text{encapsulation}}$  of the encapsulation layer, the diffusivity ratio  $D_{\text{encapsulation}}/D$ , and initial thickness ratio  $h_{\text{encapsulation}}/h_0$ . Because the diffusivity ratio  $D_{\text{encapsulation}}/D$  is much smaller than 1, the water concentration in Mg is relatively uniform whereas that in MgO is not (Fig. 3(b)). In comparison to Fig. 3(a), the water concentration in Mg increases much slower, which effectively extends the lifetime of Mg.

In the same manner as described in the previous section, the remaining thickness  $h$  of the Mg layer normalized by its initial thickness  $h_0$  is obtained as

$$\frac{h}{h_0} = 1 - \frac{w_0 M}{q \rho M_{\text{H}_2\text{O}}} k \left[ Gt \cdot \frac{\sinh \sqrt{\frac{kh_0^2}{D}}}{\sqrt{\frac{kh_0^2}{D}}} + \sum_{n=1}^{\infty} \frac{C_n}{\lambda_n} (1 - e^{-\lambda_n t}) \frac{\sin \sqrt{\frac{\lambda_n - k}{D}} h_0}{\sqrt{\frac{\lambda_n - k}{D}}} \right. \\ \left. \times \sin \sqrt{\frac{\lambda_n - k_{\text{encapsulation}}}{D_{\text{encapsulation}}}} h_{\text{encapsulation}} \right], \quad (12)$$

where  $G$  is given in Eq. (10a). As Mg is below the MgO encapsulation layer, it is difficult to measure the thickness change of Mg. Noticing MgO is not conductive, the electric resistance of Mg (or this bi-layered structure) is then measured, from which the thickness can be calculated  $h = R_0 h_0 / R$ . To understand the thickness effect of MgO encapsulation, both 400 nm-thick and 800 nm-thick MgO layers are studied on a 300 nm-thick Mg layer. As shown in Fig. 4(c), the normalized electrical resistance  $R/R_0$  versus the normalized time  $Dt/h_0^2$  predicted from the theory agrees well with the experimental measurements. A comparison between two Mg + MgO structure layouts indicates a substantial increase in the dissolution time as the thickness of encapsulation layer increases. This comes from the fact that the diffusion of water in MgO is much slower than that in Mg, which effectively extends the lifetime of Mg in providing an effective way to control the dissolution time.

The summation on the right hand side of Eq. (12) is negligible for devices relevant to transient implants. As a result, the thickness decreases linearly with time. The simple and approximate expression is given as  $h/h_0 \approx 1 - t/t'_c$ , where

$$t'_c = \frac{t_c}{G \cosh \sqrt{\frac{kh_0^2}{D}}} = t_c \left( \sqrt{\frac{kD}{k_{\text{encapsulation}} D_{\text{encapsulation}}}} \tanh \sqrt{\frac{kh_0^2}{D}} \sinh \xi + \cosh \xi \right) \quad (13)$$

is the critical time for complete physical disappearance of the Mg conductor layer in the device and  $t_c$  is the critical time in the single-layer system. From the remaining thickness  $h$ , the rate of dissolution can be solved as  $v_{\text{dissolution}} = -dh/dt \approx h_0/t'_c$ . The rate of dissolution is approximately linear with the initial thickness  $h_0$  and it can be further simplified for a sufficiently thin Mg layer ( $kh_0^2/D \ll 1$ ) as  $v_{\text{dissolution}} = w_0 M / (q \rho M_{\text{H}_2\text{O}}) (kh_0 / \cosh \xi)$ .

As an alternative, silicon oxides and nitrides can also be considered as encapsulation layers in addition to their use as gate and interlayer dielectrics, as they are typically known to be barrier materials for permeation of water [11]. As a primary source of leakage for vapors or fluids, defects such as pinholes are commonly found in films of silicon oxides and nitrides. As

$$\begin{aligned}
C_n &= -\frac{\int_0^{h_0+h_{\text{encapsulation}}} f_n(y) g(y) dy}{\int_0^{h_0+h_{\text{encapsulation}}} f_n^2(y) dy} \\
&= \frac{-\frac{2}{\lambda_n} \sqrt{(\lambda_n - k_{\text{encapsulation}}) D_{\text{encapsulation}}} \cos\left(\sqrt{\frac{\lambda_n - k}{D}} h_0\right)}{\left\{ h_0 \sin^2\left(\sqrt{\frac{\lambda_n - k_{\text{encapsulation}}}{D_{\text{encapsulation}}} h_{\text{encapsulation}}}\right) \left[ 1 + \frac{\sin\left(2\sqrt{\frac{\lambda_n - k}{D}} h_0\right)}{2\sqrt{\frac{\lambda_n - k}{D}} h_0}\right] \right.} \\
&\quad \left. + h_{\text{encapsulation}} \cos^2\left(\sqrt{\frac{\lambda_n - k}{D}} h_0\right) \left[ 1 - \frac{\sin\left(2\sqrt{\frac{\lambda_n - k_{\text{encapsulation}}}{D_{\text{encapsulation}}} h_{\text{encapsulation}}}\right)}{2\sqrt{\frac{\lambda_n - k_{\text{encapsulation}}}{D_{\text{encapsulation}}} h_{\text{encapsulation}}}}\right] \right\}}.
\end{aligned} \tag{11}$$

Box I.

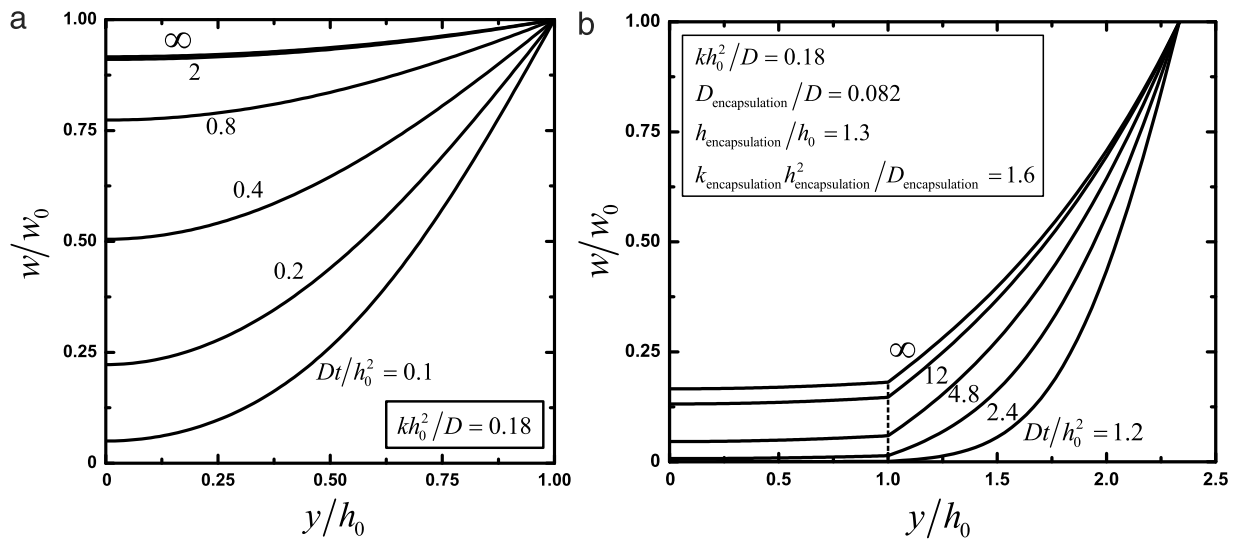


**Fig. 3.** Distribution of water concentration predicted from models of reactive diffusion for the normalized time  $Dt/h_0^2 = 0.1, 0.2, 0.4, 0.8, 2$  and  $\infty$  in (a) an Mg layer ( $kh_0^2/D = 0.18$ ) without encapsulation layer, and (b) both an Mg conductor layer encapsulated by an MgO layer ( $kh_0^2/D = 0.18$ ,  $D_{\text{encapsulation}}/D = 0.082$ ,  $h_{\text{encapsulation}}/h_0 = 1.3$ , and  $k_{\text{encapsulation}} h_{\text{encapsulation}}^2/D_{\text{encapsulation}} = 1.6$ ).  
Source: Reprinted with permission from Ref. [12].

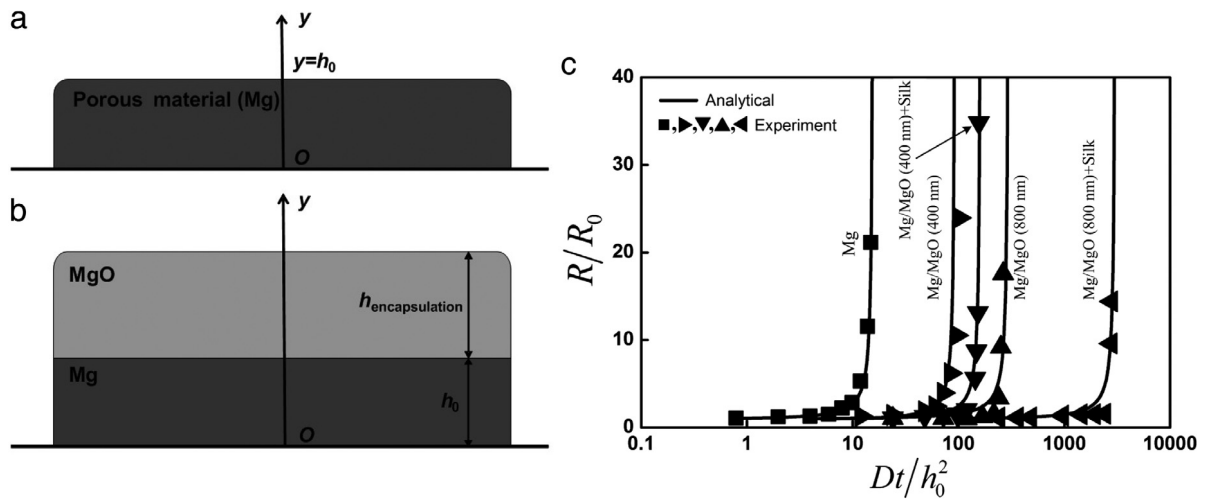


**Fig. 4.** Schematic illustrations for models of reactive diffusion and modeling predictions of the electrical resistance compared with experimental measurements. (a) Single-layered structure and (b) bi-layered structure used in models of reactive diffusion for porous materials. (c) Experimental and modeling results of the electric resistance of Mg and Mg with different encapsulation strategies (e.g., MgO encapsulation layers and/or silk overcoats).  
Source: Reprinted with permission from Ref. [12].

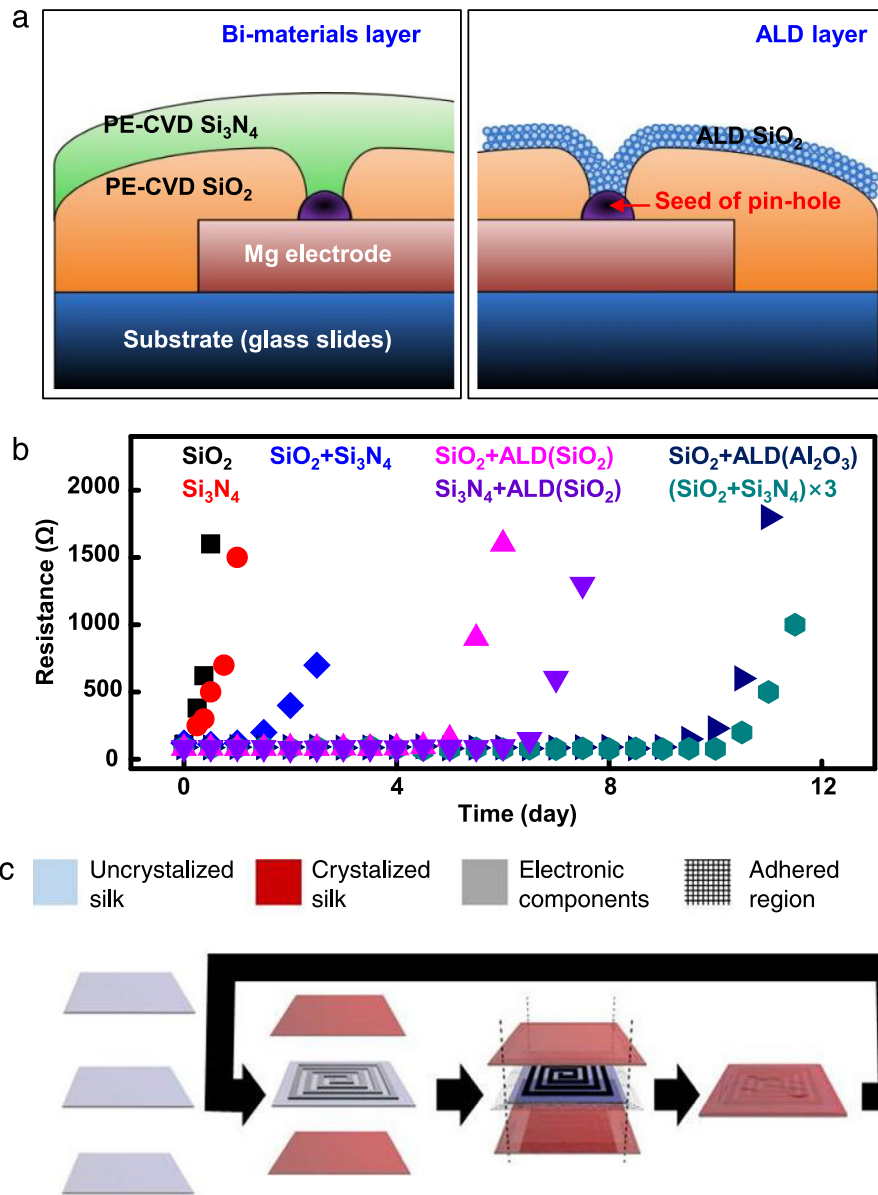


**Fig. 5.** Encapsulation strategies with multilayer structures. (a) Schematic illustrations of encapsulation methods for transient electronic devices, with defects (e.g., pinholes) covered by a bilayer of  $\text{SiO}_2/\text{Si}_3\text{N}_4$  (left) or an ALD layer (right). (b) Measurements of changes in resistance of Mg traces with an initial thickness of 300 nm encapsulated with different encapsulation approaches (in deionized water at room temperature). Encapsulation strategies examined here include a single layer of PECVD  $\text{SiO}_2$  (black, 1  $\mu\text{m}$ ), PECVD-LF  $\text{Si}_3\text{N}_4$  (red, 1  $\mu\text{m}$ ) and ALD  $\text{SiO}_2$  (orange, 20 nm); a double layer of PECVD  $\text{SiO}_2$ /PECVD-LF  $\text{Si}_3\text{N}_4$  (blue, 500/500 nm), PECVD  $\text{SiO}_2$ /ALD  $\text{SiO}_2$  (magenta, 500/20 nm), PECVD-LF  $\text{Si}_3\text{N}_4$ /ALD  $\text{SiO}_2$  (purple, 500/20 nm); and a triple layer of PECVD  $\text{SiO}_2$ /PECVD-LF  $\text{Si}_3\text{N}_4$  (Cyan, 200/200/200/200/100/100 nm). (c) Fabrication strategy for the multilayer silk pocket. Crystallization of the outer layers renders them water insoluble, whereas the inner device substrate layer can remain crystallized. Sealing the outer edges around the device encapsulates it in a protective silk pocket. Multilayer fabrication is carried out by repeating the process with an inner pocket as the device layer. (For interpretation of the references to color in this figure legend, the reader is referred to the web version of this article.)  
Source: Figure (a) (b) reprinted with permission from Ref. [11] and (c) reprinted with permission from Ref. [34].

a result, multilayer structures with different materials [11] have been developed to cooperatively eliminate defects [32] for use in transient electronics. In addition to a combination of multiple different layers, i.e.  $\text{SiO}_2$  and  $\text{Si}_3\text{N}_4$  (Fig. 5(a) left), atomic layer deposition (ALD) provides a complementary strategy to reduce defects and improve the performance of the encapsulation, even with thin layers (Fig. 5(a), right) [33]. As shown in Fig. 5(b), measured changes in resistance of a serpentine-shaped Mg trace with an initial thickness of 300 nm demonstrate the effectiveness of several encapsulation approaches.

To achieve an even longer desired lifetime for transient electronic devices, silk overcoats have also been used to provide an extra barrier for water to diffuse into MgO and Mg layers [1]. A well designed layout with both MgO encapsulation and silk

overcoat can successfully increase the lifetime of devices over hundreds of times [12]. To apply the idea of multilayer structures to silk overcoats, an encapsulation strategy of exploiting multiple air pockets has been demonstrated [34]. A scheme of this strategy is shown in Fig. 5(c). Transient electronics transferred to a silk substrate are enclosed by silk films with tunable crystalline and diffusion properties. Thermal sealing of the silk films creates a small air pocket, which provides additional protection for the device components. Iteration of this process can provide multiple silk pockets as needed. The onset of device degradation starts only when swelling of the silk protective layer collapses the air pocket in a wet environment [35].

These combined strategies in encapsulation lead to two-stage dissolution kinetics in transient electronics: (i) encapsulation



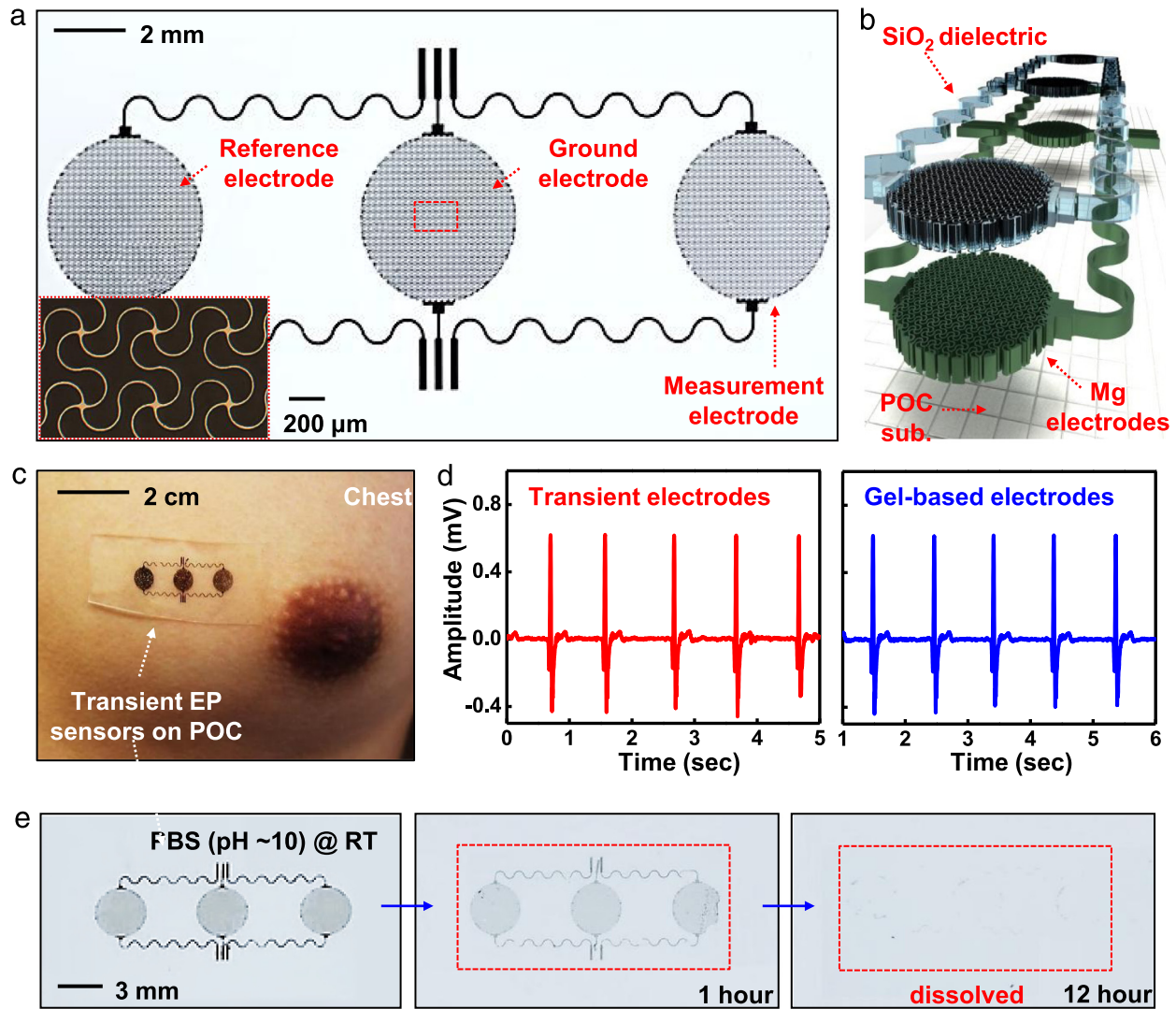


**Fig. 6.** Transient electrophysiological sensors configured in a stretchable pattern for capacitive sensing. (a) Optical image of a device and (inset) magnified view of electrode structures in the filamentary serpentine mesh layout. (b) Schematic illustration in an exploded view for the corresponding device in (a). (c) Photograph of a device mounted on the chest for measurement of electrocardiograms (ECG). (d) ECG measurements collected from transient (red) and standard gel-based (blue) devices. (e) A series of images at various dissolution stages of a transient device in PBS (pH 10) at room temperature. (For interpretation of the references to color in this figure legend, the reader is referred to the web version of this article.)

Source: Reprinted with permission from [41].

layers define the first time period of stable operation with negligible changes in electrical performance, (ii) the Mg defines the second, where the device rapidly degrades. Efficient encapsulation strategies can remove the leakage pathways and significantly increase the time for stable operation. Realizing the full potential of transient electronics for implanted applications ultimately requires conformal contact with organs of the body. To this end, a recent development of transient medical devices exploits the concepts of stretchable electronics [36–40] by use of biodegradable elastomers [41]. As shown in optical images and schematic illustrations (Fig. 6(a) and (b)), a stretchable and transient electrophysiology sensor is constructed. Thin layers of Mg (300 nm) and SiO<sub>2</sub> (100 nm) are designed in the form of filamentary serpentine meshes [42–44] (Fig. 6(a), inset) for measurement, ground and reference electrodes and connecting leads. Capacitive sensing leads to the use of a biodegradable polymer [45,46] between the Mg electrodes and the skin. The measurements show levels of fidelity comparable to those of conventional gel electrodes (Fig. 6(d)), as demonstrated in the high quality ECG measurements on the chest (Fig. 6(c)). Figure 6(e) presents a set of images of a

transient electrophysiology sensor at various dissolution stages in PBS (pH 10) at room temperature. The dissolution behavior of each component is consistent with separate studies of these materials discussed in the previous section (complete dissolution within hours for Mg or days/weeks for SiO<sub>2</sub>).

## 5. Conclusion

When exposed to bio-fluids or water, the class of silicon-based high performance transient electronics disintegrates and dissolves to eliminate the need for recollection. A number of discoveries have been made in the effort to control how transient electronics dissolve. Firstly, a number of materials, including semiconductors, and their method of application in the design of transient electronics were studied. Secondly, a model of reactive diffusion was presented to predict the way in which a component would dissolve in bio-fluids or water. This model considered a variety of factors including the porosity of the material. Thirdly, this model was extended to study the reactive diffusion in a bi-layered structure. The analytical results connect the key electrical

property to models of reactive diffusion and provide the capability to use such analytics in conjunction with established circuit simulators as a comprehensive design approach.

Since the nature of the materials used in transient electronics exhibits a decisive effect on the dissolution of resulting electronics, future material science research would be desirable. Other strategies besides encapsulation would also be worth future research to understand multiple ways of controlling the dissolution behavior of transient electronics. Active control of the transience in devices is of interest for the future development as well. Combining possibilities in transient electronics with ideas in soft, “tissue-like” devices further expands opportunities for applications in biomedicine. Overall, however, the research performed thus far on the design of transient electronics has been extensive and the potential use of this technology in industry is evident.

## Acknowledgments

H. C. was a Howard Hughes Medical Institute International Student Research fellow. The authors acknowledge the start-up fund provided by the Engineering Science and Mechanics Department, College of Engineering, and Materials Research Institute at the Pennsylvania State University (215–37 1001 cc: H. Cheng).

## References

- [1] S.-W. Hwang, H. Tao, D.-H. Kim, et al., A physically transient form of silicon electronics, *Science* 337 (2012) 1640–1644.  
<http://www.sciencemag.org/content/337/6102/1640>.
- [2] S.W. Hwang, G. Park, H. Cheng, et al., 25th anniversary article: Materials for high-performance biodegradable semiconductor devices, *Adv. Mater.* 26 (2014) 1992–2000.  
<http://onlinelibrary.wiley.com/doi/10.1002/adma.201470082/abstract>.
- [3] R.O. Darouiche, Treatment of infections associated with surgical implants, *N. Engl. J. Med.* 350 (2004) 1422–1429.  
<http://www.nejm.org/doi/full/10.1056/NEJMra035415>.
- [4] H. Tao, S.-W. Hwang, B. Marelli, et al., Silk-based resorbable electronic devices for remotely controlled therapy and in vivo infection abatement, *Proc. Natl. Acad. Sci.* 111 (2014) 17385–17389.  
<http://www.pnas.org/content/111/49/17385.abstract>.
- [5] C. Dagdeviren, S.W. Hwang, Y. Su, et al., Transient, biocompatible electronics and energy harvesters based on ZnO, *Small* 9 (2013) 3398–3404.  
<http://onlinelibrary.wiley.com/doi/10.1002/smll.201300146/abstract>.
- [6] H.L. Hernandez, S.K. Kang, O.P. Lee, et al., Triggered transience of metastable poly (phthalaldehyde) for transient electronics, *Adv. Mater.* 26 (2014) 7637–7642.  
<http://onlinelibrary.wiley.com/doi/10.1002/adma.201403045/abstract>.
- [7] C.H. Lee, S.K. Kang, G.A. Salvatore, et al., Wireless microfluidic systems for programmed, functional transformation of transient electronic devices, *Adv. Funct. Mater.* 25 (2015) 5100–5106.  
<http://onlinelibrary.wiley.com/doi/10.1002/adfm.201502192/abstract>.
- [8] C.W. Park, S.K. Kang, H.L. Hernandez, et al., Thermally triggered degradation of transient electronic devices, *Adv. Mater.* 27 (2015) 3783–3788.  
<http://onlinelibrary.wiley.com/doi/10.1002/adma.201501180/abstract>.
- [9] X. Huang, Y. Liu, S.W. Hwang, et al., Biodegradable materials for multilayer transient printed circuit boards, *Adv. Mater.* 26 (2014) 7371–7377.  
<http://onlinelibrary.wiley.com/doi/10.1002/adma.201403164/abstract>.
- [10] S.W. Hwang, S.K. Kang, X. Huang, et al., Materials for programmed, functional transformation in transient electronic systems, *Adv. Mater.* 27 (2015) 47–52.  
<http://onlinelibrary.wiley.com/doi/10.1002/adma.201403051/abstract>.
- [11] S.K. Kang, S.W. Hwang, H. Cheng, et al., Dissolution behaviors and applications of silicon oxides and nitrides in transient electronics, *Adv. Funct. Mater.* 24 (2014) 4427–4434.  
<http://onlinelibrary.wiley.com/doi/10.1002/adfm.201304293/abstract>.
- [12] R. Li, H. Cheng, Y. Su, et al., An analytical model of reactive diffusion for transient electronics, *Adv. Funct. Mater.* 23 (2013) 3106–3114.  
<http://onlinelibrary.wiley.com/doi/10.1002/adfm.201203088/abstract>.
- [13] C.J. Bettinger, Z. Bao, Organic thin-film transistors fabricated on resorbable biomaterial substrates, *Adv. Mater.* 22 (2010) 651–655.  
<http://onlinelibrary.wiley.com/doi/10.1002/adma.200902322/abstract>.
- [14] M. Irimia-Vladu, P.A. Troshin, M. Reisinger, et al., Biocompatible and biodegradable materials for organic field-effect transistors, *Adv. Funct. Mater.* 20 (2010) 4069–4076.  
<http://onlinelibrary.wiley.com/doi/10.1002/adfm.201001031/abstract>.
- [15] F. Eder, H. Klauk, M. Halik, et al., Organic electronics on paper, *Appl. Phys. Lett.* 84 (2004) 2673–2675.  
<http://scitation.aip.org/content/aip/journal/apl/84/14/10.1063/1.1690870>.
- [16] D.H. Kim, Y.S. Kim, J. Amsden, et al., Silicon electronics on silk as a path to bioresorbable, implantable devices (vol 95, 133701, 2009), *Appl. Phys. Lett.* 95 (2009).  
<http://scitation.aip.org/content/aip/journal/apl/95/13/10.1063/1.3238552>.
- [17] S.-K. Kang, G. Park, K. Kim, et al., Dissolution chemistry and biocompatibility of silicon- and Germanium-based semiconductors for transient electronics, *ACS Appl. Mater. Interfaces* 7 (2015) 9297–9305.  
<http://pubs.acs.org/doi/abs/10.1021/acsami.5b02526>.
- [18] J.D. Rimstidt, H.L. Barnes, The kinetics of silica–water reactions, *Geochim. Cosmochim. Acta* 44 (1980) 1683–1699.  
<http://www.sciencedirect.com/science/article/pii/0016703780902203>.
- [19] H. Seidel, L. Csepregi, A. Heuberger, et al., Anisotropic etching of crystalline silicon in Alkaline-solutions. 1. Orientation dependence and behavior of passivation layers, *J. Electrochem. Soc.* 137 (1990) 3612–3626.  
<http://jes.ecsdl.org/content/137/11/3612>.
- [20] S.-W. Hwang, G. Park, C. Edwards, et al., Dissolution chemistry and biocompatibility of single-crystalline silicon nanomembranes and associated materials for transient electronics, *ACS Nano* 8 (2014) 5843–5851.  
<http://pubs.acs.org/doi/abs/10.1021/nn500847g>.
- [21] H. Seidel, L. Csepregi, A. Heuberger, et al., Anisotropic etching of crystalline silicon in Alkaline-solutions. 2. Influence of dopants, *J. Electrochem. Soc.* 137 (1990) 3626–3632.  
<http://jes.ecsdl.org/content/137/11/3612>.
- [22] L. Yin, A.B. Farimani, K. Min, et al., Mechanisms for hydrolysis of silicon nanomembranes as used in bioresorbable electronics, *Adv. Mater.* 27 (2015) 1857–1864.  
<http://onlinelibrary.wiley.com/doi/10.1002/adma.201404579/abstract>.
- [23] P.V. Danckwerts, Absorption by simultaneous diffusion and chemical reaction, *Trans. Faraday Soc.* 46 (1950) 300.  
<http://pubs.rsc.org/en/Content/ArticleLanding/1950/TF/TF9504600300#ldivAbstract>.
- [24] I.A. Taub, W. Roberts, S. LaGambina, et al., Mechanism of dihydrogen formation in the magnesium–water reaction? *J. Phys. Chem. A* 106 (2002) 8070–8078.  
<http://pubs.acs.org/doi/abs/10.1021/jp0143847>.
- [25] L. Yin, H. Cheng, S. Mao, et al., Dissolvable metals for transient electronics, *Adv. Funct. Mater.* 24 (2014) 645–658.  
<http://onlinelibrary.wiley.com/doi/10.1002/adfm.201301847/abstract>.
- [26] H. Inoue, K. Sugahara, A. Yamamoto, et al., Corrosion rate of magnesium and its alloys in buffered chloride solutions, *Corros. Sci.* 44 (2002) 603–610.  
<http://www.sciencedirect.com/science/article/pii/S0010938X01000920>.
- [27] W. Ng, K. Chiu, F. Cheng, Effect of pH on the *i* in vitro corrosion rate of magnesium degradable implant material, *Mater. Sci. Eng. C* 30 (2010) 898–903.  
<http://www.sciencedirect.com/science/article/pii/S0928493110000895>.
- [28] G. Wirth, J. Gieskes, The initial kinetics of the dissolution of vitreous silica in aqueous media, *J. Colloid Interface Sci.* 68 (1979) 492–500.  
<http://www.sciencedirect.com/science/article/pii/0021979779903072>.
- [29] W.G. Worley, Dissolution Kinetics and Mechanisms in Quartz- and Granite-Water Systems, Massachusetts Institute of Technology, 1994.  
<http://dspace.mit.edu/handle/1721.1/28068>.
- [30] M. Pourbaix, Atlas of Electrochemical Equilibria in Aqueous Solutions, 1974.
- [31] J.P. Hoare, Oxide film studies on iron in electrochemical machining electrolytes, *J. Electrochem. Soc.* 117 (1970) 142–145.  
<http://jes.ecsdl.org/content/117/1/142.abstract>.
- [32] J. Rosink, H. Lifka, G. Rietjens, et al., 34.1: Ultra-thin encapsulation for large-area OLED displays. Paper Presented at: SID Symposium Digest of Technical Papers, Wiley Online Library, 2005.  
<http://onlinelibrary.wiley.com/doi/10.1889/1.2036236/abstract>.
- [33] J. Meyer, P. Görrn, F. Bertram, et al., Al<sub>2</sub>O<sub>3</sub>/ZrO<sub>2</sub> nanolaminates as ultrahigh gas-diffusion barriers—A strategy for reliable encapsulation of organic electronics, *Adv. Mater.* 21 (2009) 1845–1849.  
<http://onlinelibrary.wiley.com/doi/10.1002/adma.200803440/abstract>.
- [34] M.A. Brenckle, H. Cheng, S. Hwang, et al., Modulated degradation of transient electronic devices through multilayer silk fibroin pockets, *ACS Appl. Mater. Interfaces* (2015).  
<http://pubs.acs.org/doi/abs/10.1021/acsami.5b06059?journalCode=aamick>.
- [35] B.D. Lawrence, S. Wharram, J.A. Kluge, et al., Effect of hydration on silk film material properties, *Macromol. Biosci.* 10 (2010) 393–403.  
<http://www.ncbi.nlm.nih.gov/pubmed/20112237>.
- [36] H. Cheng, Y. Zhang, K.-C. Hwang, et al., Buckling of a stiff thin film on a prestrained bi-layer substrate, *Int. J. Solids Struct.* 51 (2014) 3113–3118.  
<http://www.sciencedirect.com/science/article/pii/S002076831400198X>.
- [37] H. Cheng, J. Wu, M. Li, et al., An analytical model of strain isolation for stretchable and flexible electronics, *Appl. Phys. Lett.* 98 (2011) 061902.  
<http://scitation.aip.org/content/aip/journal/apl/98/6/10.1063/1.3553020>.
- [38] D.-H. Kim, N. Lu, R. Ma, et al., Epidermal electronics, *Science* 333 (2011) 838–843.  
<https://www.sciencemag.org/content/333/6044/838.abstract>.
- [39] J.A. Rogers, T. Someya, Y.G. Huang, Materials and mechanics for stretchable electronics, *Science* 327 (2010) 1603–1607.  
<http://www.sciencemag.org/content/327/5973/1603.abstract>.
- [40] J. Viventi, D.H. Kim, J.D. Moss, et al., A conformal, bio-interfaced class of silicon electronics for mapping cardiac electrophysiology, *Sci. Transl. Med.* 2 (2010) 838–843.  
<http://pubs.acs.org/doi/abs/10.1021/jp0143847>.
- [41] S.-W. Hwang, C.H. Lee, H. Cheng, et al., Biodegradable elastomers and silicon nanomembranes/nanoribbons for stretchable, transient electronics, and biosensors, *Nano Lett.* 15 (2015) 2801–2808.  
<http://pubs.acs.org/doi/abs/10.1021/nl503997m>.
- [42] D.H. Kim, J.L. Xiao, J.Z. Song, et al., Stretchable, curvilinear electronics based on inorganic materials, *Adv. Mater.* 22 (2010) 2108–2124.  
<http://onlinelibrary.wiley.com/doi/10.1002/adma.200902927/abstract>.

- [43] D.H. Kim, J.H. Ahn, W.M. Choi, et al., Stretchable and foldable silicon integrated circuits, *Science* 320 (2008) 507–511.  
<http://www.sciencemag.org/content/320/5875/507>.
- [44] R.H. Kim, M.H. Bae, D.G. Kim, et al., Stretchable, transparent graphene interconnects for arrays of microscale inorganic light emitting diodes on rubber substrates, *Nano Lett.* 11 (2011) 3381–3886.  
<http://pubs.acs.org/doi/abs/10.1021/nl202000u>.
- [45] S.W. Hwang, J.K. Song, X. Huang, et al., High-performance biodegradable/transient electronics on biodegradable polymers, *Adv. Mater.* 26 (2014) 3905–3911.  
<http://onlinelibrary.wiley.com/doi/10.1002/adma.201306050/abstract>.
- [46] J. Yang, A.R. Webb, G.A. Ameer, Novel citric acid-based biodegradable elastomers for tissue engineering, *Adv. Mater.* 16 (2004) 511–516.  
<http://onlinelibrary.wiley.com/doi/10.1002/adma.200306264/abstract>.